5 Element Strategy Initiative to Form Core Research Center for Electron Materials

– Multi-probe study using synchrotron light, neutron, and muon beams –

Youichi Murakami, Hiroshi Kumigashira,
Ryosuke Kadono, Jun-ichi Yamaura

5-1 Introduction

The national project “Elements strategy initiative to form core research centers” was launched in 2012, aiming to develop entirely new materials based on ubiquitous elements. The research was conducted primarily at four research centers, which were established in research institutes and universities. They carry out studies on (1) magnetic materials, (2) electronic materials, (3) catalysts and batteries, and (4) structural materials. This project is connected to the research center for electronic materials of the Tokyo Institute of Technology. We have put much effort into evaluating and analyzing new materials, establishing material concepts, and developing techniques for evaluating materials using synchrotron light, neutron, and muon beams. We report the year’s main topics: polar nano-region (PNR) structure in $LaTiO_2N$, electronic structure of hydrogen in IGZO, and anionic electron-induced magnetism in Y_2C.

5-2 Polar nano-region structure in the oxynitride perovskite $LaTiO_2N$

Oxynitride perovskites with an AMX_3 structure (A = alkali earth metal, rare earth; M = Ti, Zr, Nb, Ta, W; X = O, N) are emerging materials that hold promise as visible-light responsive photocatalysts and chromatically tunable nontoxic pigments [1-3]. The ability to modify their electronic states by replacing oxygen with nitrogen has gained attention, particularly as candidates for lead-free dielectric materials that are stable in air and water. The interplay between the structure and the mechanisms is expected to be revealed.

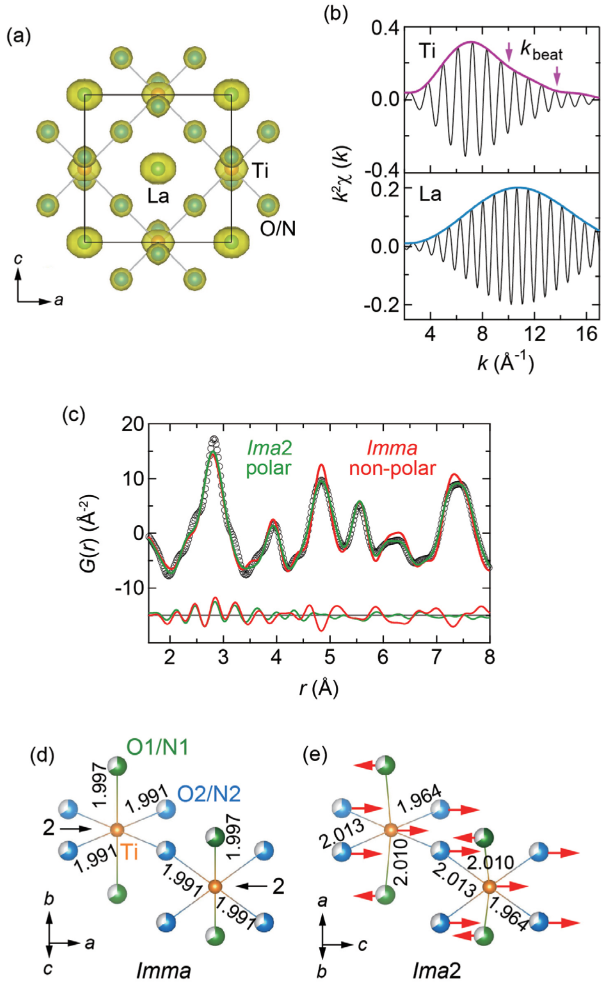

Fig. 1: (a) The isosurface of MEM electron density for $LaTiO_2N$. (b) Fourier-filtered EXAFS oscillations and amplitudes for Ti (upper panel) and La (lower panel). Kinks exist at k_{beat} = 10.0 and 13.8 Å^{-1} in the Ti profile, as indicated by the arrows. (c) PDF data (black circles) in the range of 1.6-8 Å. The lower curves are the difference profiles between the experimental data and the calculated patterns. (d, e) Average (*Imma*) and nano-region (*Ima*2) structure for $LaTiO_2N$. The arrows indicate the relative displacements from the *Imma* average structure.

We present average and local structure analyses of $LaTiO_2N$ through synchrotron X-ray diffraction (XRD) measurements at PF BL-8B, extended X-ray absorption fine-structure (EXAFS) at PF-AR NW10A, and atomic pair distribution function (PDF) from neutron total scattering at J-PARC BL-21 NOVA.

From the MEM calculation based on the XRD data, elongated electron densities were found, suggesting anisotropic displacements from the equilibrium position along the a-axis (Fig. 1(a)) [4]. Fig. 1(b) plots the Fourier-filtered EXAFS oscillations and amplitudes for La-Ti and La-La shells [4]. We found kinks, as indicated by the arrows, at k_{beat} ~ 10.0 and 13.8 $Å^{-1}$ in the La-Ti shell. The kink stems from the beat from the phase difference of EXAFS oscillations along with different bond distances ΔR in the shell. Based on the relation $\Delta R = \pi/(2k_{beat})$, we can estimate the ΔR of the La-Ti bond distances to be $\Delta R = 0.16$ and 0.11 Å, which are unknown distortions in the *Imma* structure.

We proceeded to a multiscale data treatment through PDF analysis from the neutron total scattering data. In the medium-range region ($8 < r < 20$ Å), we could refine the structure of the *Imma* structure [4]. In the short-range region (Fig. 1c, $1.6 < r < 8$ Å), we succeeded in refining the structure according to *Ima*2 symmetry. These results show that the crystal structure of $LaTiO_2N$ can be regarded as polar *Ima*2 at the nanoscale and nonpolar *Imma* in the average structure (Figs. 1(d) and 1(e)).

The observed polar structure in nanoscale bears a resemblance to PNR formation in the relaxor. Unlike these cases for a classical PMN relaxor, the PNR in $LaTiO_2N$ can most likely be ascribed in terms of short-range O/N cis-order. Taking into account the ferroelectric material in general exhibits high permittivity due to its large polarization, the PNR may be closely tied to the high permittivity in $LaTiO_2N$.

5-3 Electronic structure of hydrogen in In-Ga-Zn-O semiconductor simulated by muon

In-Ga-Zn oxide, widely known as IGZO, is a semiconductor used as a channel material in transparent thin-film transistors (TFTs) for display applications. IGZO has properties superior to those of conventional Si TFTs, such as relatively high electron mobility, low-temperature fabrication over a large area, uniformity, and stability. However, there are some remaining issues for amorphous IGZO (a-IGZO), including negative bias illumination stress (NBIS) instability. NBIS instability refers to a negative shift of the threshold voltage in the normal operation condition in which TFTs are always illuminated by the backlight under a negative bias voltage. The microscopic mechanism of this instability is still under debate.

It is known that various electronic properties of IGZO are influenced by hydrogen (H) in small amounts. For instance, water vapor annealing improves the carrier mobility and the S-value (sharpness of the TFT switching as a function of gate-source voltage). Strong n-type conductivity is induced by H treatment, suggesting the occurrence of a shallow donor state (see Fig. 2). Recent infrared transmission spectroscopy has revealed the subgap state near the valence band maximum arising from two hydride ions at the oxygen vacancy ($2H^-$ at V_O) [5, 6]. It is argued that this subgap state is associated with the NBIS mechanism; thus, understanding the microscopic details of these processes would be crucial in controlling and stabilizing the electronic properties of IGZO.

We were thus motivated to investigate the local electronic structure of interstitial H in IGZO using the muon spin rotation (μSR) technique. Implanted muon mimics the behavior of interstitial

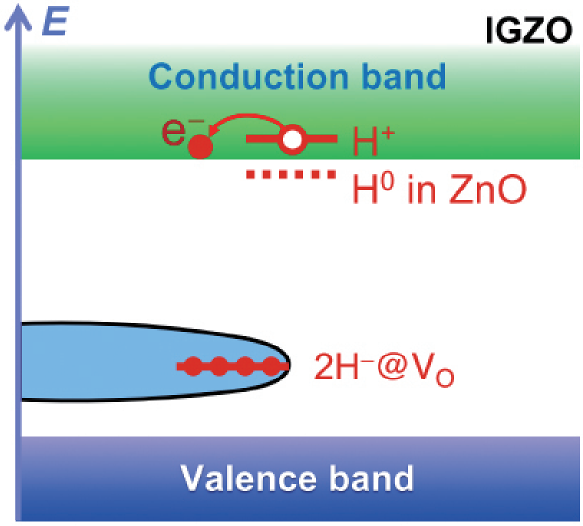

Fig. 2: A schematic diagram of the energy band structure for IGZO, where hydrogen-related electronic levels suggested by earlier studies are shown.

H in matter, and it can be regarded as pseudo-H. We have proposed the designation muogen (Mu) as the elemental name [7], where the charge states of muogen, Mu^+, Mu_0, and Mu^- correspond to those of H^+, H_0, and H^-, respectively. (Note that the term "muonium" specifically refers to the atomic structure corresponding to Mu^0, not to the properties as an element.)

Conventional μSR measurements on crystalline IGZO (c-IGZO) were performed using the ARTEMIS spectrometer at MUSE of MLF J-PARC. Meanwhile, μSR measurements on amorphous (a-) IGZO and hydrogenated a-IGZO (a-IGZO:H) thin films were performed using a low-energy muon (LEM) beam at the Paul Scherrer Institute, Switzerland. Muon stopping profiles for c-IGZO films (5.97 g/cm^3) are shown in Fig. 2(d), where most of the LEM measurements were performed at 11 keV LEM.

Figures 3(a) and 3(b) show the typical zero-field (ZF) spectra of c-IGZO and as-deposited a-IGZO, respectively [8]. Each ZF spectrum exhibits slow Gaussian damping with partial recovery of polarization at later time domains (t ≥ 10 μs). Spectra were analyzed using the following expressions:

$$A_0 P_\mu(t) = A_s G_{\mathrm{KT}}(\Delta, t) + A_{\mathrm{BG}} \qquad (1)$$

$$G_{\mathrm{KT}}(\Delta, t) = \frac{1}{3} + \frac{2}{3}\left[1 - (\Delta t)^2\right] \exp\left[-\frac{1}{2}(\Delta t)^2\right],$$

where $P_\mu(t)$ represents the time evolution of the muon spin polarization in the sample and the sample holder with their respective partial asymmetry being A_s and A_{BG} ($A_0 = A_s + A_{BG}$). $G_{KT}(\Delta, t)$ is the static Kubo-Toyabe relaxation function, with the term Δ representing the local field distribution caused by nuclear magnetic moments around the muon site(s). As shown by the solid curves in Fig. 3(a), the spectra were perfectly reproduced by Eq. (1), indicating that muons are entirely in the diamagnetic state (Mu^+ and/or Mu^-). It is apparent from the longitudinal field (LF) spectra in c-IGZO that Mu senses the quasistatic field distribution. The temperature dependence of Δ obtained by curve-fitting is shown in Fig. 3(c).

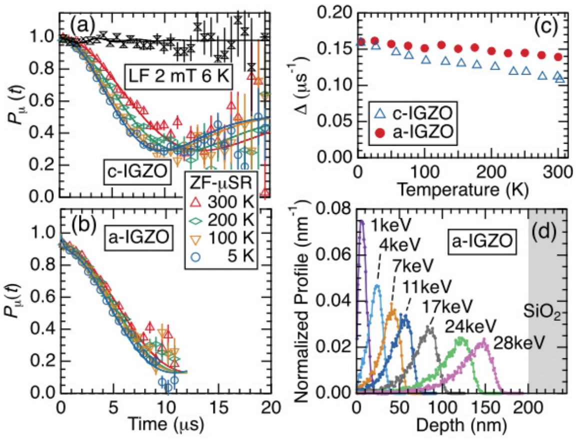

Fig. 3: μSR time spectra for (a) c-IGZO and (b) as-deposited a-IGZO [8]. (c) Temperature dependence of Δ. (d) Muon stopping profiles for respective implantation energies.

Candidate Mu sites were narrowed down by simulation:

(1) DFT calculation for H (to mimic Mu) using the VASP code to estimate the structural relaxation around H and the formation energy E_f with some initial structures around H owing to the random occupation of Ga and Zn in their crystallographically equivalent sites.

(2) Calculation of Δ at H site in their converged structure.

The calculated E_f and Δ are shown in Fig.4. It is noticeable that Δ reduces with decreasing E_f, and the number of Ga and In ions around Mu grows with increasing E_f. This indicates that H prefers the Ga/Zn-O layer to the InO_2 layer and that H sites are stabilized by a Zn-rich structure.

The inset in Fig. 4 represents the local structure around H for Zn^4O^4. Structural similarity to ZnO suggests that the local electronic structure of

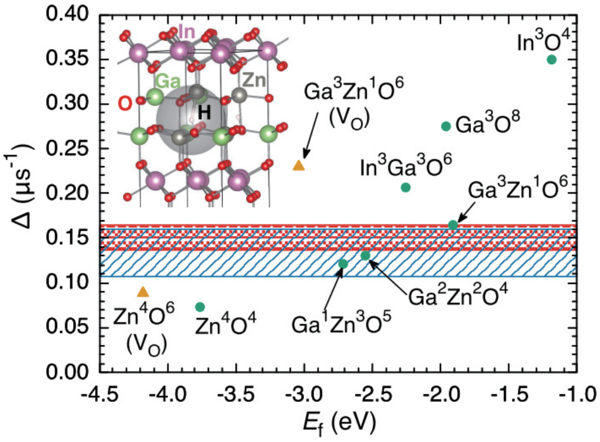

Fig. 4: E_f and Δ for the candidate Mu sites, where label $A^iB^jC^k$ indicates the element name and number of atoms located within 0.3 nm from Mu. V_o means Mu at an oxygen vacancy site. The hatched areas represent the range of Δ for c-IGZO (blue) and a-IGZO (red). Inset shows the local structure around H for Zn^4O^4. A large gray sphere represents the region of 0.3 nm from H.

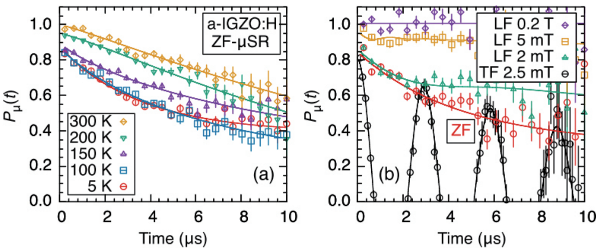

Fig. 5: (a) Temperature dependence of ZF spectra in a-IGZO:H. (b) TF, ZF, and LF spectra measured at 5 K.

Mu/H is similar to that in ZnO, where Mu^0 is presumed to be localized at the bond center of Zn-O.

Meanwhile, the situation in the hydrogenated film turned out to be qualitatively different from the pristine film. As shown in Fig. 5(a), the initial muon polarization is missing at lower temperatures $[P_\mu(t = 0) < 1]$. The remaining component exhibited a slow exponential-like depolarization. The transverse field (TF) and LF spectra, shown in Fig. 5(b), reveal that the depolarization is due to a static local field with a Lorentzian distribution exerting diamagnetic Mu. These features strongly suggest that the distance between Mu and the nuclear magnetic moments is not uniform, in contrast with the pristine films. This leads to the presumption that another H atom may be located around the Mu site in a-IGZO:H, which also invokes a model of $2H^-$ at VO proposed by recent studies [5, 6].

5-4 Anionic electron-induced magnetism in a two-dimensional electride Y_2C: inelastic neutron scattering study

Electrides are ionic crystals in which electrons serve as anions. In contrast to the nearly free electrons in a metal, the anionic electrons in the electrides are loosely bound at the interstitial space. This leads to a significantly low work function of the materials. Because of this property, electrides have provided a fertile field of remarkable applications, such as electron injection layers in organic light-emitting diodes and catalysts for ammonia synthesis.

Y_2C is reported to be a two-dimensional electride [9]. Since the standard valence states of Y and C are Y^{3+} and C^{4-}, two excess electrons are expected to exist in the interlayer of $[Y_2C]^{2+}$, as shown in Fig. 6(a) to preserve charge neutrality. Magnetism arising from anionic electrons has been a fundamental issue since the discovery of organic electrides in the 1980s. Among the reported electrides, Y_2C shows curious magnetic features. Theoretically, Y_2C is expected to be a weak itinerant ferromagnet or close to a ferromagnetic instability, and a small magnetic moment is induced as a result of the hybridization between the Y 4d and the anionic s-like orbitals [10]. Recently, using the muon spin rotation/relaxation (µSR) technique, it was shown that the Curie-Weiss-like behavior is intrinsic to the electronic state of the sample [11]. To verify these expectations, we performed inelastic neutron scattering experiments for an identical batch of polycrystalline Y_2C used in the previous µSR study.

Figure 6(b) shows the neutron scattering intensities of polycrystalline Y_2C as a function of the momentum transfer Q and energy transfer E. A slight but a clear scattering around Q = 0 $Å^{-1}$ can be observed at both temperatures 7 and 120 K. Intensities of these scatterings are 3 orders smaller than those of elastic scatterings and depend on temperature. Although an intensity from phonon scatterings increases with Q2, acoustic phonon signals standing from the 003 Bragg point around Q = 1.05 $Å^{-1}$ are absent in such a low Q region. Therefore, these subtle scatterings can be attributed to a magnetic origin. On the other hand, no magnetic ordering was observed down to 7 K. These results strongly support the theoretically suggested magnetic state of Y_2C; namely, Y_2C has a ferromagnetic instability.

The E dependence of the observed intensities

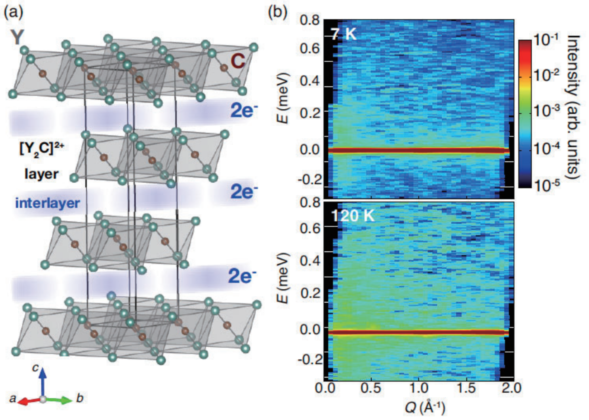

Fig. 6: (a) Crystal structure of Y_2C together with schematics of an anionic electron layer. Solid lines indicate the conventional hexagonal unit cell. (b) Neutron scattering spectra of polycrystalline Y_2C at 7 and 120 K as a function of the momentum transfer Q and the energy transfer E. A color gauge showing the strength of intensities in a logarithmic scale.

for several Q regions at 7 and 120 K is well described by a Lorentzian form, which is adopted in the self-consistent renormalization (SCR) theory for itinerant weak ferromagnets [12]. This fitting procedure gives spatial correlation lengths of 26 Å at 7 K and 10 Å at 120 K. It is worth mentioning here that the existence of the spatial magnetic correlation indicates that the observed magnetic excitations in Y_2C originate not from magnetic impurities, but the intrinsic electronic state of Y_2C. Using these correlation lengths, we can plot the inverse lifetime of spin fluctuation as a function of the wave number, which is predicted by the SCR theory. The agreement was satisfactory. From these results, we found that the SCR theory works well to explain the magnetic excitation of Y_2C.

In summary, we performed an inelastic neutron scattering experiment to investigate anionic electron-induced magnetism in polycrystalline Y_2C. We successfully observed a ferromagnetic spin fluctuation over a wide temperature range. This result suggests that the ferromagnetic spin fluctuation plays a dominant role in the magnetism in Y_2C. Therefore, the SCR theory would be appropriate for a description of the Curie-Weiss-like behavior of the magnetic susceptibility of Y_2C.

References

[1] Oxynitride Perovskites: Synthesis and Structures of $LaZrO_2N$, $NdTiO_2N$, and $LaTiO_2N$ and Comparison with Oxide Perovskites, S. J. Clarke, B. P. Guinot, C. W. Michie, M. J. C. Calmont and M. Rosseinsky, Chem. Mater., **14**, 288 (2002).

[2] High-Temperature Synthesis and Structures of Perovskite and n = 1 Ruddlesden–Popper Tantalum Oxynitrides, S. J. Clarke, K. A. Hardstone, C. W. Michie and M. Rosseinsky, Chem. Mater., **14**, 2664 (2002).

[3] Characterization of the Structural, Optical, and Dielectric Properties of Oxynitride Perovskites AMO_2N (A = Ba, Sr, Ca; M = Ta, Nb), Y. I. Kim, P. M. Woodward, K. Z. Baba-Kishi and C. W. Tai, Chem. Mater., **16**, 1267 (2004).
M. Jansen and H. P. Letschert, Nature, **404**, 980 (2000).

[4] Polar nano-region structure in the oxynitride perovskite $LaTiO_2N$, J. Yamaura, S. Maki, T. Honda, Y. Matsui, A. Noviyanto, T. Otomo, H. Abe, Y. Murakami, and N. Ohashi, Chem. Commun., **56**, 1385 (2020).

[5] Hydrogen anion and subgap states in amorphous In–Ga–Zn–O thin films for TFT applications, J. Bang, S. Matsuishi, and H. Hosono, Appl. Phys. Lett. **110**, 232105 (2017).

[6] Hydrogen and the Light-Induced Bias Instability Mechanism in Amorphous Oxide Semiconductors., H. Li, Y. Guo, and J. Robertson, Sci. Rep. **7**, 16858 (2017).

[7] Local electronic structure of interstitial hydrogen in iron disulfide, H. Okabe, M. Hiraishi, S. Takeshita, A. Koda, K. M. Kojima, and R. Kadono, Phys. Rev. B. **98**, 075210 (2018).

[8] Electronic structure of interstitial hydrogen in In-Ga-Zn-O semiconductor simulated by muon, K. M. Kojima, M. Hiraishi, A. Koda, R. Kadono, K. Ide, S. Matsuishi, H. Kumomi, T. Kamiya, and H. Hosono, Appl. Phys. Lett. **115**, 122104 (2019).

[9] Two-Dimensional Transition-Metal Electride Y_2C, X. Zhang, Z. Xiao, H. Lei, Y. Toda, S. Matsuishi, T. Kamiya, S. Ueda, and H. Hosono, Chem. Mat., **26**, 6638 (2014).

[10] Ferromagnetic instability of interlayer floating electrons in the quasi-two-dimensional electride Y_2C, T. Inoshita, N. Hamada, and H. Hosono, Phys. Rev. B **92**, 201109 (2015).

[11] Electronic correlation in the quasi-two-dimensional electride Y_2C, M. Hiraishi, K. M. Kojima, I. Yamauchi, H. Okabe, S. Takeshita, A. Koda, R. Kadono, X. Zhang, S. Matsuishi, H. Hosono, K. Hirata, S. Otani, and N. Ohashi, Phys. Rev. B **98**, 041104 (2018).

[12] Spin Fluctuations in Itinerant Electron Magnetism, T. Moriya, (Springer-Verlag, Berlin) (1895).